MDPI

Anharmonic Vibrational Frequencies of Water Borane and Associated Molecules

Brent R. Westbrook [ID] and Ryan C. Fortenberry *[ID]

Department of Chemistry & Biochemistry, University of Mississippi, University, MS 38677, USA;
bwestbr2@go.olemiss.edu
* Correspondence: r410@olemiss.edu

Abstract: Water borane (BH_3OH_2) and borinic acid (BH_2OH) have been proposed as intermediates along the pathway of hydrogen generation from simple reactants: water and borane. However, the vibrational spectra for neither water borane nor borinic acid has been investigaged experimentally due to the difficulty of isolating them in the gas phase, making accurate quantum chemical predictions for such properties the most viable means of their determination. This work presents theoretical predictions of the full rotational and fundamental vibrational spectra of these two potentially application-rich molecules using quartic force fields at the CCSD(T)-F12b/cc-pCVTZ-F12 level with additional corrections included for the effects of scalar relativity. This computational scheme is further benchmarked against the available gas-phase experimental data for the related borane and HBO molecules. The differences are found to be within 3 cm^{-1} for the fundamental vibrational frequencies and as close as 15 MHz in the B_0 and C_0 principal rotational constants. Both BH_2OH and BH_3OH_2 have multiple vibrational modes with intensities greater than 100 km mol^{-1}, namely ν_2 and ν_4 in BH_2OH, and ν_1, ν_3, ν_4, ν_9, and ν_{13} in BH_3OH_2. Finally, BH_3OH_2 has a large dipole moment of 4.24 D, which should enable it to be observable by rotational spectroscopy, as well.

Keywords: vibrational spectroscopy; anharmonic frequencies; rotational spectroscopy; quantum chemistry; alternative fuels; coupled cluster theory; hydrogen production

1. Introduction

Borane-containing molecules like ammonia borane are promising hydrogen storage media for use in fuel cells due to their high hydrogen density [1–4]. However, all of this storage capacity is of little use without a clean way to liberate the hydrogen into hydrogen gas. To this end, recent work has revived an interest in borane as a feedstock for generating hydrogen gas from water that dates back at least to the 1950s [5,6]. Combining borane [7] or diborane [5,7] with water can produce substantial amounts of hydrogen gas, which is becoming increasingly important as a source of alternative fuels [6,8–11]. Current methods of producing hydrogen gas, however, still rely primarily upon fossil fuels, limiting the clean nature of the resulting hydrogen [7]. As shown previously [6,7], an important step along the hydrogen production pathway when using borane feedstocks is the formation of BH_3OH_2 or water borane. This can then decompose with a submerged barrier into one equivalent of hydrogen gas and borinic acid, BH_2OH. Such a pathway suggests that borane and its hydrated or ammonia-complexed variants may have a substantial role to play not only in the storage of large amounts of hydrogen but also in the generation of hydrogen from water.

Limiting the optimism surrounding such promise is the difficulty of isolating and then conclusively identifying individual borane complexes in the gas phase. Such identification is of the utmost necessity given the fact that borane tends to form dative bonds that are exquisitely sensitive to the surrounding environment [12,13]. In ammonia borane, in particular, this spectroscopic sensitivity has led theoretical work on the ammonia borane dimer to show shifts of up to 40 cm^{-1} in the B-N stretching frequency from the isolated

molecule [12]. Similarly, IR and Raman experiments exhibit even larger shifts of up to 150 cm^{-1} in the solid phase [14,15]. While previous work has demonstrated that boron forms stronger bonds to oxygen than it does to nitrogen [16], these bonds will likely still be dative and preserve the same sensitivity observed in the B-N bond of ammonia borane. In both cases, this behavior means these molecules, and the boron-heavy atom stretching frequency in particular, can also serve as indicators of their environmental conditions. Better knowledge of these conditions may help to inform designers of water splitting catalysts of the H$_2$-producing mechanism. For these indicators to be useful, however, there must be highly accurate, benchmark vibrational data for the isolated molecules.

Unfortunately, the same sensitivity that makes such data appealing also increases the difficulty of obtaining it experimentally. As a result, theoretical investigations are the best chance for obtaining accurate vibrational data for these sensitive frequencies. Previous work [13] on ammonia borane demonstrates agreement in the computed values to within 5 cm^{-1} of the seven available gas-phase vibrational frequencies [4] and offers a new theoretical prediction of the B-N stretching frequency that continues to elude experimental detection.

The previous work on ammonia borane [13] utilizes a quartic force field (QFF) methodology combined with coupled cluster theory at the singles, doubles, and perturbative triples level [17] within the F12 explicitly correlated construction (CCSD(T)-F12b) [18,19] and a triple-ζ basis set. Such a method and basis set combination is commonly abbreviated as F12-TZ. QFFs are fourth-order Taylor series expansions of the internuclear potential energy portion of the Watson Hamiltonian [20]. When coupled with the F12-TZ level of theory, QFFs frequently offer agreement with gas-phase vibrational frequencies of within 5 to 7 cm^{-1} [21–25]. Other techniques for computing accurate anharmonic spectral data exist [26], but as a result of the good performance of the F12-TZ QFF on ammonia borane, this same methodology is used herein to investigate water borane (BH$_3$OH$_2$), borinic acid (BH$_2$OH), HBO, and borane (BH$_3$).

One shortcoming of the F12-TZ methodology is its inability to produce very accurate rotational constants [22–24]. When accurate rotational data is needed, much more expensive composite QFFs have often been employed that achieve agreement of about 20 MHz in the vibrationally-averaged ground state rotational constants [27]. Chief among these composite methods is CcCR, which is composed of a complete basis set extrapolation ("C"), corrections for core correlation ("cC"), and corrections for scalar relativity ("R") [20]. However, recent work [28] has explored the use of a hybrid between F12-TZ and CcCR, fittingly referred to as F12-TZ-cCR. This method utilizes CCSD(T)-F12b with the cc-pCVTZ-F12 basis set, explicit treatment of core electrons, and the same correction for scalar relativity as CcCR. It offers more accurate rotational constants with agreement on the order of 7.5 MHz with experimental data while still capturing an order-of-magnitude decrease in the computational cost relative to CcCR [28]. As such, this methodology is also employed herein to offer better predictions of the rotational spectra of these molecules.

While water borane and borinic acid do not have existing gas-phase infrared data, the related borane and HBO molecules do. Kawaguchi et al. have reported high-resolution vibrational frequencies for borane [29], and Kawashima et al. have determined both rotational and vibrational experimental data for HBO [30]. In both cases, these data will help to benchmark the accuracy of the theoretical results presented herein on the structurally similar water borane and borinic acid molecules. Borinic acid also has some available rotational constants [31] that will further help to contextualize the rotational data reported here, as well.

2. Computational Details

The F12-TZ and F12-TZ-cCR computations performed in the present work, including geometry optimizations, harmonic frequencies, dipoles, and single-point energies, all utilize the Molpro 2020.1 software package [32]. All of the F12-TZ computations solely use the cc-pVTZ-F12 basis set [21,33,34], while the F12-TZ-cCR geometry optimizations

require the cc-pCVTZ-F12 basis set [34]. The F12-TZ-cCR single-point energy computations additionally utilize canonical CCSD(T) with a cc-pVTZ-DK basis set to account for the effects of scalar relativity [35,36]. Double-harmonic and anharmonic infrared intensities are computed within the Gaussian16 suite of programs [37] using the MP2/aug-cc-pVTZ level of theory [38,39]. The harmonic values at this level of theory have been previously shown to yield semi-quantitative accuracy in the infrared intensities, and the differences from the anharmonic values are typically negligible [40–42].

For both the F12-TZ and F12-TZ-cCR QFFs, following the geometry optimization, displacements of 0.005 Å or radians are taken from the optimized geometry to map out the QFF. The symmetry internal coordinates (SICs) along which these displacements are taken are shown below for BH_3OH_2 with atom labels corresponding to Figure 1.

$$S_1(a') = r(H_1 - B_2) \tag{1}$$

$$S_2(a') = r(B_2 - O_3) \tag{2}$$

$$S_3(a') = \frac{1}{\sqrt{2}}[r(B_2 - H_4) + r(B_2 - H_5)] \tag{3}$$

$$S_4(a') = \frac{1}{\sqrt{2}}[r(O_3 - H_6) + r(O_3 - H_7)] \tag{4}$$

$$S_5(a') = \angle(H_1 - B_2 - O_3) \tag{5}$$

$$S_6(a') = \frac{1}{\sqrt{2}}[\angle(H_5 - B_2 - O_3) + \angle(H_4 - B_2 - O_3)] \tag{6}$$

$$S_7(a') = \frac{1}{\sqrt{2}}[\angle(H_6 - O_3 - B_2) + \angle(H_7 - O_3 - B_2)] \tag{7}$$

$$S_8(a') = \frac{1}{\sqrt{2}}[\tau(H_1 - B_2 - O_3 - H_6) - \tau(H_1 - B_2 - O_3 - H_7)] \tag{8}$$

$$S_9(a') = \frac{1}{\sqrt{2}}[\tau(H_5 - B_2 - O_3 - H_6) - \tau(H_4 - B_2 - O_3 - H_7)] \tag{9}$$

$$S_{10}(a'') = \frac{1}{\sqrt{2}}[r(B_2 - H_4) - r(B_2 - H_5)] \tag{10}$$

$$S_{11}(a'') = \frac{1}{\sqrt{2}}[r(O_3 - H_6) - r(O_3 - H_7)] \tag{11}$$

$$S_{12}(a'') = \frac{1}{\sqrt{2}}[\angle(H_5 - B_2 - O_3) - \angle(H_4 - B_2 - O_3)] \tag{12}$$

$$S_{13}(a'') = \frac{1}{\sqrt{2}}[\angle(H_6 - O_3 - B_2) - \angle(H_7 - O_3 - B_2)] \tag{13}$$

$$S_{14}(a'') = \frac{1}{\sqrt{2}}[\tau(H_1 - B_2 - O_3 - H_6) + \tau(H_1 - B_2 - O_3 - H_7)] \tag{14}$$

$$S_{15}(a'') = \frac{1}{\sqrt{2}}[\tau(H_5 - B_2 - O_3 - H_6) + \tau(H_4 - B_2 - O_3 - H_7)] \tag{15}$$
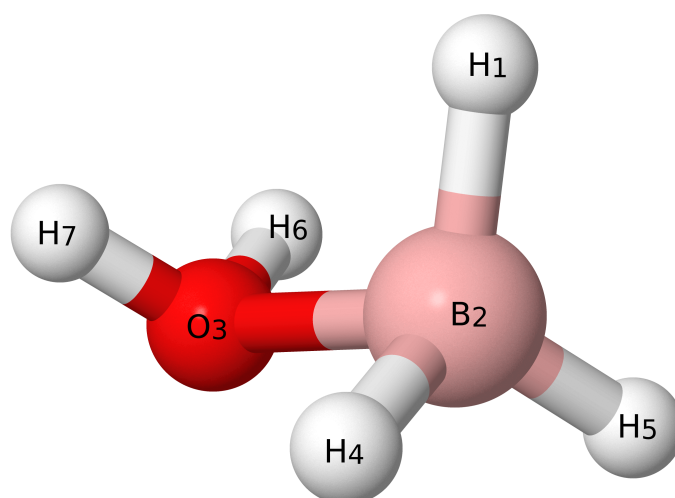
Figure 1. Visual depiction of BH_3OH_2.

Similarly, the SICs for borinic acid with atom labels given by Figure 2 are
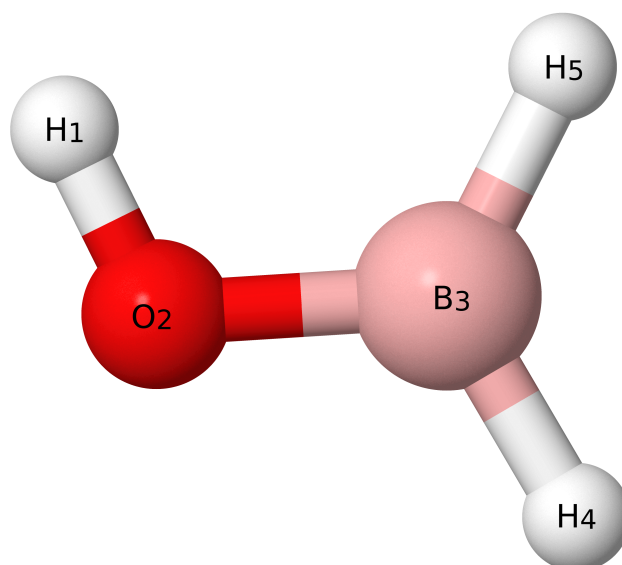
Figure 2. Visual depiction of borinic acid.

$$
\begin{align}
S_1(a') &= r(H_1 - O_2) \tag{16} \\
S_2(a') &= r(O_2 - B_3) \tag{17} \\
S_3(a') &= r(B_3 - H_4) \tag{18} \\
S_4(a') &= r(B_3 - H_5) \tag{19} \\
S_5(a') &= \angle(H_1 - O_2 - B_3) \tag{20} \\
S_6(a') &= \angle(O_2 - B_3 - H_4) \tag{21} \\
S_7(a') &= \angle(O_2 - B_3 - H_5) \tag{22} \\
S_8(a'') &= \tau(H_1 - O_2 - B_3 - H_4) \tag{23} \\
S_9(a'') &= \tau(H_1 - O_2 - B_3 - H_5), \tag{24}
\end{align}
$$

Those for HBO with atom labels from Figure 3 are
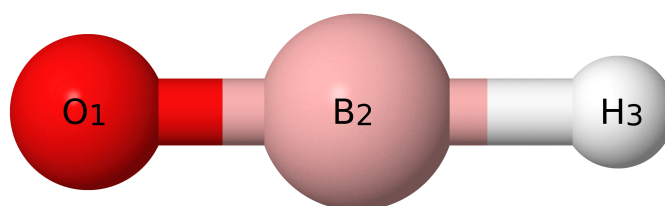
Figure 3. Visual depiction of HBO.

$$S_1(\sigma) \quad = \quad r(O_1 - B_2) \tag{25}$$

$$S_2(\sigma) \quad = \quad r(B_2 - H_3) \tag{26}$$

$$S_3/S_4(\pi) \quad = \quad \angle(O_1 - B_2 - H_3), \tag{27}$$

And those for borane with atom labels from Figure 4 are
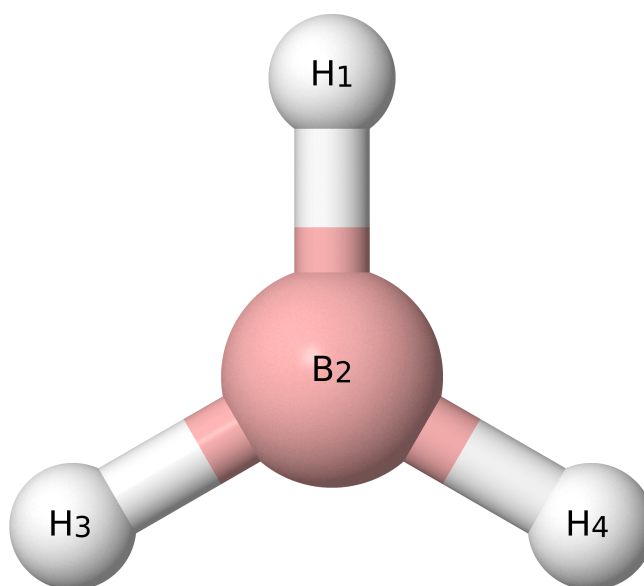
Figure 4. Visual depiction of borane.

$$S_1(a_1) \quad = \quad r(H_1 - B_2) \tag{28}$$

$$S_2(a_1) \quad = \quad \frac{1}{\sqrt{2}}[r(B_2 - H_3) + r(B_2 - H_4)] \tag{29}$$

$$S_3(a_1) \quad = \quad \frac{1}{\sqrt{2}}[\angle(H_1 - B_2 - H_3) + \angle(H_1 - B_2 - H_4)] \tag{30}$$

$$S_4(b_2) \quad = \quad \frac{1}{\sqrt{2}}[r(B_2 - H_3) - r(B_2 - H_4)] \tag{31}$$

$$S_5(b_2) \quad = \quad \frac{1}{\sqrt{2}}[\angle(H_1 - B_2 - H_3) - \angle(H_1 - B_2 - H_4)] \tag{32}$$

$$S_6(b_1) \quad = \quad \text{OUT}(H_1 - B_2 - H_3 - H_4). \tag{33}$$

As shown by the symmetry labels in Equations (28)–(33), borane is treated in C_{2v} symmetry rather than its full D_{3h} symmetry to simplify the coordinate system. The SIC coordinate systems utilized herein for BH_3OH_2 and BH_2OH have been previously applied to the structurally similar AlH_3OH_2 [43] and AlH_2OH [44] molecules, respectively. The total numbers of single-point energy computations to generate the QFFs for BH_3OH_2, BH_2OH, BH_3, and HBO are 19585, 3161, 413, and 55.

After the single-point energy computations for either QFF energy, the QFF function is fit using a least-squares procedure with sums of squared residuals on the order of 10^{-16} a.u.^{2}

in all cases. The first fit yields the equilibrium geometries and a subsequent refitting zeroes the gradients and produces a new equilibrium geometry along with the corresponding force constants. These force constants are transformed from SICs to Cartesian coordinates using the INTDER program [45]. The Cartesian force constants are then utilized by the second-order rotational and vibrational perturbation theory [46] implementations in the SPECTRO software package [47] to generate the rovibrational spectral data [48,49]. Type 1 and 2 Fermi resonances, Fermi polyads [50], Coriolis resonances, and Darling-Dennison resonances are taken into account to further increase the accuracy of the rovibrational data [50,51]. The Fermi resonances are listed in the Supplementary Information (SI) in Tables S4, S6, S8, S10, S12, S14, S24, S28, S34, S40, S47 and S54. Additionally, the rotational constants from the SPECTRO program are used in the PGOPHER software package [52] to simulate the rotational and rovibrational spectra for BH_2OH and BH_3OH_2 shown in Figures 5–8.

3. Results and Discussion

3.1. Benchmarks

As shown in Tables 1 and 2, the F12-TZ-cCR QFF fundamental frequencies demonstrate excellent agreement with the available gas-phase experimental data. In the case of borane, the largest difference occurs in ν_3 with a deviation of only 1.9 cm^{-1}, and the mean absolute error (MAE) or unsigned averaged deviation across the three modes is 1.1 cm^{-1}. This is in contrast to the F12-TZ results, which are a bit farther from the experimental values. Again for borane, the biggest deviation from experiment in the F12-TZ results is 7.5 cm^{-1} with an MAE of 3.8 cm^{-1}. The two are more comparable for HBO, where F12-TZ achieves a respectable MAE of 3.9 cm^{-1} relative to the two available experimental frequencies. However, F12-TZ-cCR still has the slight edge with an MAE of 2.8 cm^{-1}. Such performance indicates that both F12-TZ and F12-TZ-cCR can adequately handle the vibrational spectra of these two molecules, but for a slight increase (3484 versus 5397 seconds of wall time for BH_3) in computational cost, F12-TZ-cCR provides a substantial increase in accuracy.

Table 1. Harmonic and anharmonic vibrational frequencies (in cm^{-1}), MP2/aug-cc-pVTZ harmonic and anharmonic infrared intensities (in km mol^{-1}, labeled f), equilibrium, vibrationally averaged, and singly-vibrationally excited principal rotational constants (in MHz), and dipole (in D) for HBO. Descriptions of the vibrational frequencies are given as linear combinations of SICs and as qualitative descriptions along with the symmetries.

	SICs	Description	Symmetry	f	F12-TZ	F12-TZ-cCR	Expt. [a]
ω_1	$0.932S_2 - 0.068S_1$	B-H stretch	σ	4	2890.3	2897.6	
ω_2	$0.932S_1 + 0.068S_2$	B-O stretch	σ	35	1837.8	1845.8	
ω_3	$0.500S_3 + 0.500S_4$	H-B-O bend	π	12	764.6	764.9	
ZPVE					3098.4	3111.3	
ν_1	$0.932S_2 - 0.068S_1$	B-H stretch	σ	4	2779.5	2795.2	
ν_2	$0.932S_1 + 0.068S_2$	B-O stretch	σ	33	1822.8	1829.5	1825.5610
ν_3	$0.500S_3 + 0.500S_4$	H-B-O bend	π	11	749.4	756.1	754.4163
B_e					39,198.2	39,411.0	39,400.668
B_0					39,026.3	39,238.6	39,224.247
B_1					38,757.3	38,967.4	
B_2					38,767.3	38,978.0	
B_3					39,118.3	39,331.9	
μ						2.74	

[a] From Ref. [30].

Table 2. Harmonic and anharmonic vibrational frequencies (in cm^{-1}), MP2/aug-cc-pVTZ harmonic and anharmonic infrared intensities (in km mol^{-1}, labeled f), equilibrium, vibrationally averaged, and singly-vibrationally excited principal rotational constants (in MHz), and dipole (in D) for BH_3. Descriptions of the vibrational frequencies are given as linear combinations of SICs and as qualitative descriptions along with the symmetries.

	SICs	Description	Symmetry	f	F12-TZ	F12-TZ-cCR	Expt. [a]
ω_1	$0.334S_1 - 0.167S_2 + 0.501S_4$	antisymm. stretch	b_2	133	2700.3	2708.5	
ω_2	$0.667S_2 + 0.333S_1$	symm. stretch	a_1	0	2567.6	2575.0	
ω_3	$0.501S_5 + 0.501S_3$	in-plane rock	b_2	17	1218.4	1221.4	
ω_4	$1.000S_6$	out-of-plane wag	b_1	90	1156.9	1159.9	
ZPVE					5724.1	5740.6	
ν_1	$0.334S_1 - 0.167S_2 + 0.501S_4$	antisymm. stretch	b_2	135	2594.0	2601.9	2601.5779
ν_2	$0.667S_2 + 0.333S_1$	symm. stretch	a_1	0	2498.4	2505.8	
ν_3	$0.501S_5 + 0.501S_3$	in-plane rock	b_2	17	1194.9	1197.9	1196.0217
ν_4	$1.000S_6$	out-of-plane wag	b_1	86	1144.9	1148.7	1147.49087
B_e					236,255.9	237,314.5	
C_e					118,127.8	118,657.3	
B_0					235,210.3	236,268.5	236,071.4
C_0					115,831.7	116,349.1	116,283.5
B_1					233,018.6	234,064.7	234,104.0
C_1					114,910.4	115,422.2	115,411.0
B_2					233,201.4	234,248.8	
C_2					114,827.3	115,339.3	
B_3					238,431.6	239,513.3	23,9112.4
C_3					114,665.5	115,177.1	11,5130.0
B_4					233,068.4	234,113.6	23,4801.4
C_4					116,418.6	116,940.3	116,643.1
D_J					17.016	17.160	18.199
D_{JK}					−29.579	−29.834	−32.746
D_K					13.676	13.795	15.46
$H_J \times 10^3$					3.476	3.521	3.639
$H_{JK} \times 10^3$					−12.606	−12.771	−14.48
$H_{KJ} \times 10^3$					14.853	15.047	17.898
$H_K \times 10^3$					−5.711	−5.786	−7.081
μ					0.00		

[a] From Ref. [29].

The same is true upon examination of the principal rotational constants. While F12-TZ-cCR exhibits fairly large deviations from the experimental data for borane giving an overall MAE of 218.3 MHz, F12-TZ performs much worse with an MAE of 750.2 MHz. This is in line with previous work on both F12-TZ [22–24] and F12-TZ-cCR [28], which demonstrates that accounting for the effects of core correlation in F12-TZ-cCR is necessary for producing more accurate rotational constants. In the present case, neither of the methodologies utilized herein seems to be achieving real accuracy, but F12-TZ-cCR still has a clear advantage. For HBO, that advantage becomes even more pronounced. Whereas F12-TZ has an MAE from the reported B_e and B_0 values of 200.2 MHz, F12-TZ-cCR achieves a much more reasonable MAE of only 12.3 MHz. Looking at the vibrationally-averaged B_0 value tells the same story; the F12-TZ QFF differs from the experimental value by 197.9 MHz and the F12-TZ-cCR value by only 14.4 MHz. Differently, both F12-TZ and F12-TZ-cCR seem to capture the quartic and sextic distortion coefficients in the Watson S-reduced Hamiltonian presented at the bottom of Table 2. The two computational data sets agree very closely with each other in this case. Neither is more than 3 MHz away in the D constants (−32.746 compared to −29.834 MHz for D_{JK}) or 3 kHz in the H constants (17.898 compared to 15.047 kHz for H_{KJ}) from the available borane experimental values, and most of the differences are even smaller.

Finally, but perhaps most promisingly, the same trend is clear in the borinic acid data shown in Table 3. Compared to the available experimental vibrationally-averaged rotational constants, F12-TZ has an MAE difference of 308.7 MHz. In stark contrast, F12-TZ-cCR manages an MAE of only 22.3 MHz, and most of this is concentrated in the difference from A_0 of 66.0 MHz. The F12-TZ-cCR values for both B_0 and C_0 agree to within just over

0.5 MHz. Such exceptional agreement even exceeds the expected performance of F12-TZ-cCR, which previously achieved an average agreement of roughly 7.5 MHz on similar B_0 and C_0 rotational constants [28]. This suggests that F12-TZ-cCR is very well suited to the determination of the vibrational spectrum of borinic acid and for the elucidation of both the rotational and vibrational spectra of water borane. The accuracy of the rotational constants in the case of water borane is particularly important given its massive dipole moment of 4.24 D, which should make its rotational spectrum easier to obtain if the molecule itself can be isolated experimentally.

Table 3. Harmonic and anharmonic vibrational frequencies (in cm^{-1}), MP2/aug-cc-pVTZ harmonic and anharmonic infrared intensities (in km mol^{-1}, labeled f), equilibrium, vibrationally averaged, and singly-vibrationally excited principal rotational constants (in MHz), and dipole (in D) for BH_2OH. Descriptions of the vibrational frequencies are given as linear combinations of SICs and as qualitative descriptions along with the symmetries.

	SICs	Description	Symmetry	f	F12-TZ	F12-TZ-cCR	Expt. [a]
ω_1	$1.000S_1$	O-H stretch	a'	83	3867.8	3869.8	
ω_2	$0.739S_3 - 0.260S_4$	B-H antisymm. stretch	a''	172	2673.2	2679.9	
ω_3	$0.739S_4 + 0.259S_3$	B-H symm. stretch	a'	104	2572.8	2579.4	
ω_4	$0.568S_2 - 0.247S_7 - 0.182S_6$	B-O stretch	a'	151	1376.7	1382.0	
ω_5	$0.577S_5 - 0.273S_7 + 0.099S_6 - 0.050S_2$	H-O-B bend	a'	6	1190.9	1194.0	
ω_6	$0.412S_6 + 0.380S_2 + 0.167S_7$	H-B-O bend	a'	112	1188.2	1192.4	
ω_7	$0.559S_9 - 0.441S_8$	out-of-plane wag	a''	51	1061.9	1065.1	
ω_8	$0.381S_5 + 0.314S_7 - 0.308S_6$	in-plane rock	a'	57	894.0	897.8	
ω_9	$0.559S_8 + 0.441S_9$	torsion	a''	83	785.4	789.3	
ZPVE					7708.4	7725.5	
ν_1	$1.000S_1$	O-H stretch	a'	77	3681.1	3683.0	
ν_2	$0.739S_3 - 0.260S_4$	B-H antisymm. stretch	a''	169	2555.6	2561.6	
ν_3	$0.739S_4 + 0.259S_3$	B-H symm. stretch	a'	76	2456.2	2462.4	
ν_4	$0.568S_2 - 0.247S_7 - 0.182S_6$	B-O stretch	a'	152	1347.7	1352.8	
ν_5	$0.577S_5 - 0.273S_7 + 0.099S_6 - 0.050S_2$	H-O-B bend	a'	22	1154.1	1158.3	
ν_6	$0.412S_6 + 0.380S_2 + 0.167S_7$	H-B-O bend	a'	98	1167.8	1171.1	
ν_7	$0.559S_9 - 0.441S_8$	out-of-plane wag	a''	50	1048.1	1051.4	
ν_8	$0.381S_5 + 0.314S_7 - 0.308S_6$	in-plane rock	a'	59	880.7	882.8	
ν_9	$0.559S_8 + 0.441S_9$	torsion	a''	82	753.5	751.0	
A_e					172,890.0	173,612.5	
B_e					30,552.4	30,704.1	
C_e					25,964.1	26,090.0	
A_0					171,969.4	172,687.1	17,2621.1
B_0					30,319.5	30,469.7	30,470.22
C_0					25,689.0	25,813.1	25,812.73
A_1					170,127.7	170,835.2	
B_1					30,294.4	30,444.4	
C_1					25,631.6	25,755.3	
A_2					170,798.0	171,510.7	
B_2					30,278.4	30,428.3	
C_2					25,646.5	25,770.4	
A_3					170,001.1	170,709.4	
B_3					30,306.0	30,456.1	
C_3					25,638.0	25,761.7	
A_4					172,528.1	173,243.9	
B_4					30,328.9	30,477.1	
C_4					25,515.1	25,637.8	
A_5					175,303.8	176,002.0	
B_5					30,366.7	30,511.9	
C_5					25,594.4	25,712.3	
A_6					172,698.2	173,646.6	
B_6					30,278.2	30,437.8	
C_6					25,601.6	25,730.7	
A_7					170,201.5	170,730.6	
B_7					30,086.2	30,232.3	

Table 3. *Cont.*

	SICs	Description	Symmetry	f	F12-TZ	F12-TZ-cCR	Expt. [a]
C_7					25,724.7	25,849.0	
A_8					176,655.6	177,443.9	
B_8					30,274.3	30,423.6	
C_8					25,610.4	25,733.9	
A_9					167,569.6	168,210.5	
B_9					30,196.4	30,346.5	
C_9					25,689.4	25,813.5	
μ					1.51		1.506

[a] From Ref. [31].

3.2. Spectroscopic Data

In light of the performance of the F12-TZ-cCR QFFs on HBO, borane, and the rotational constants of borinic acid, as well as the lack of experimental data on the vibrational frequencies of borinic acid and water borane, the F12-TZ-cCR fundamental frequencies reported herein are the most accurate values available for these two molecules. In some cases, such as the high-frequency O-H stretches, the good agreement between F12-TZ and F12-TZ-cCR adds further support to the theoretical quantification of these frequencies. Across BH_3OH_2 and BH_2OH, the deviations in these frequencies are all less than 4 cm^{-1} with the largest difference occurring in ν_1 of BH_3OH_2 at 3.9 cm^{-1}. However, the B-H stretches are less consistent between the levels of theory. The ν_3 antisymmetric B-H stretch of BH_3OH_2, for example, exhibits a difference of 12.1 cm^{-1} between F12-TZ and F12-TZ-cCR. The agreement is better across the board for BH_2OH, but the ν_2 antisymmetric B-H stretch still exhibits a difference of 6.0 cm^{-1} between the two treatments. Properly handling this mode is particularly important in light of its high intensity for both molecules. In both cases, the antisymmetric B-H stretch is the most intense mode, with that of BH_2OH having an intensity of 169 km mol^{-1} and that of BH_3OH_2 even more intense at 206 km mol^{-1}.

Table 4. Harmonic and anharmonic vibrational frequencies (in cm^{-1}), MP2/aug-cc-pVTZ harmonic and anharmonic infrared intensities (in km mol^{-1}, labeled f), equilibrium, vibrationally averaged, and singly-vibrationally excited principal rotational constants (in MHz), and dipole (in D) for BH_3OH_2. Descriptions of the vibrational frequencies are given as linear combinations of SICs and as qualitative descriptions along with the symmetries.

	SICs	Description	Symmetry	f	F12-TZ	F12-TZ-cCR
ω_1	$1.000S_{11}$	antisymm. O-H stretch	a''	151	3889.9	3892.5
ω_2	$1.001S_4$	symm. O-H stretch	a'	56	3789.2	3792.0
ω_3	$1.002S_{10}$	antisymm. B-H stretch	a''	215	2586.8	2593.6
ω_4	$0.623S_3 - 0.378S_1$	symm. B-H stretch	a'	218	2556.1	2562.9
ω_5	$0.624S_1 + 0.378S_3$	B-H breathing	a'	55	2482.1	2488.7
ω_6	$0.723S_8 - 0.285S_7$	H-O-H bend	a'	92	1653.8	1655.0
ω_7	$0.663S_{14} - 0.305S_{15}$	B-H in-plane rock	a''	13	1208.4	1211.7
ω_8	$0.574S_9 + 0.278S_5 + 0.181S_6$	B-H in-plane bend	a'	29	1200.4	1204.1
ω_9	$0.462S_6 - 0.438S_9 + 0.145S_5$	B-H out-of-plane wag	a'	131	1194.6	1198.3
ω_{10}	$0.670S_{12} - 0.320S_{13}$	torsion	a''	13	1025.9	1031.4
ω_{11}	$0.503S_5 - 0.344S_6 - 0.098S_7 - 0.057S_9$	O-H wag	a'	56	952.3	957.4
ω_{12}	$0.675S_{13} + 0.296S_{12}$	antisymm. B-O-H bend	a''	3	647.3	651.4
ω_{13}	$0.629S_7 + 0.311S_8 + 0.083S_5 + 0.057S_9$	symm. B-O-H bend	a'	177	607.2	610.4
ω_{14}	$1.037S_2$	B-O stretch	a'	84	467.0	472.1
ω_{15}	$0.695S_{15} + 0.299S_{14}$	torsion	a''	39	156.4	158.1
ZPVE					11,981.3	12,050.8
ν_1	$1.000S_{11}$	antisymm. O-H stretch	a''	133	3700.9	3704.8
ν_2	$1.001S_4$	symm. O-H stretch	a'	48	3612.6	3615.6
ν_3	$1.002S_{10}$	antisymm. B-H stretch	a''	206	2476.3	2488.4
ν_4	$0.623S_3 - 0.378S_1$	symm. B-H stretch	a'	135	2444.9	2452.3
ν_5	$0.624S_1 + 0.378S_3$	B-H breathing	a'	94	2433.5	2441.2
ν_6	$0.723S_8 - 0.285S_7$	H-O-H bend	a'	60	1627.8	1634.3
ν_7	$0.663S_{14} - 0.305S_{15}$	B-H in-plane rock	a''	12	1178.2	1179.4
ν_8	$0.574S_9 + 0.278S_5 + 0.181S_6$	B-H in-plane bend	a'	23	1172.3	1175.5
ν_9	$0.462S_6 - 0.438S_9 + 0.145S_5$	B-H out-of-plane wag	a'	139	1169.0	1176.8
ν_{10}	$0.670S_{12} - 0.320S_{13}$	torsion	a''	13	944.9	971.9

Table 4. *Cont.*

	SICs	Description	Symmetry	f	F12-TZ	F12-TZ-cCR
ν_{11}	$0.503S_5 - 0.344S_6 - 0.098S_7 - 0.057S_9$	O-H wag	a'	34	898.9	927.2
ν_{12}	$0.675S_{13} + 0.296S_{12}$	antisymm. B-O-H bend	a''	1	609.4	619.4
ν_{13}	$0.629S_7 + 0.311S_8 + 0.083S_5 + 0.057S_9$	symm. B-O-H bend	a'	179	543.9	528.4
ν_{14}	$1.037S_2$	B-O stretch	a'	82	397.1	399.4
ν_{15}	$0.695S_{15} + 0.299S_{14}$	torsion	a''	35	92.1	241.2
A_e					87,262.1	87,643.7
B_e					17,819.1	17,935.7
C_e					17,330.7	17,440.4
A_0					86,509.6	86,912.3
B_0					17,143.2	17,269.0
C_0					16,699.3	16,816.4
A_1					86,052.2	86,451.9
B_1					17,149.6	17,274.8
C_1					16,716.3	16,832.9
A_2					85,973.9	86,373.0
B_2					17,147.4	17,272.8
C_2					16,701.5	16,818.2
A_3					86,275.9	86,681.7
B_3					17,212.6	17,338.0
C_3					16,762.2	16,878.9
A_4					85,874.1	86,271.5
B_4					17,229.3	17,354.6
C_4					16,768.6	16,885.2
A_5					85,926.2	86,325.9
B_5					17,193.6	17,319.1
C_5					16,754.8	16,871.6
A_6					86,341.9	86,745.4
B_6					17,166.0	17,292.6
C_6					16,679.8	16,796.9
A_7					88,456.0	89,000.3
B_7					17,140.2	17,265.6
C_7					16,727.6	16,845.1
A_8					84,427.7	84,908.1
B_8					17,124.3	17,239.7
C_8					16,675.4	16,786.5
A_9					85,882.3	86,067.2
B_9					17,111.5	17,248.4
C_9					16,649.4	16,759.4
A_{10}					87,344.8	87,759.8
B_{10}					16,917.6	17,046.2
C_{10}					16,453.6	16,586.5
A_{11}					86,365.5	86,750.3
B_{11}					16,885.5	17,012.9
C_{11}					16,485.5	16,604.8
A_{12}					87,566.4	87,974.7
B_{12}					16,989.2	17,117.7
C_{12}					16,514.9	16,634.0
A_{13}					86,943.7	87,346.7
B_{13}					16,960.9	17,088.5
C_{13}					16,516.0	16,634.8
A_{14}					86,280.7	86,678.2
B_{14}					16,619.7	16,744.1
C_{14}					16,201.6	16,317.7
A_{15}					86,427.9	86,887.0
B_{15}					16,951.3	17,088.7
C_{15}					16,616.6	16,743.7
μ					4.24	

For BH_2OH, the ν_4 B-O stretch at 1352.8 cm^{-1} is the next most intense mode with a value of 152 km mol^{-1}. The additional hydrogens in BH_3OH_2 damp both the frequency and intensity of the B-O stretch, decreasing the frequency to 399.4 cm^{-1} and the intensity to 82 km mol^{-1} in ν_{14}. This frequency is considerably lower than the previously computed value for the B-N stretch in ammonia borane at 644 cm^{-1}, but the intensity is much greater than the 12 km mol^{-1} reported therein [13]. Such a shift suggests that the B-O

bond in BH_3OH_2 is actually weaker than the B-N bond in ammonia borane, and this is corroborated by the slightly longer 1.74485 Å B-O bond length compared to the 1.67308 Å B-N bond. These expected trends in the bond strengths are supported by F12-TZ bond strength computations, which give a value of -9.7 kcal mol^{-1} for the B-O bond and -25.7 kcal mol^{-1} for the B-N bond. In contrast, the B-H bonds of BH_3OH_2 are slightly shorter at 1.20516 Å compared to the 1.21685 Å observed for ammonia borane, and this is again consistent with the higher frequency B-H stretches observed in the present work.

Examining the rest of the anharmonic infrared intensities for BH_2OH reveals that all but the ν_5 B-O-H bend have intensities greater than 50 km mol^{-1}, and even ν_5 itself still has an intensity of 22 km mol^{-1}. BH_3OH_2, on the other hand, has more low intensity fundamental vibrational frequencies, such as ν_7, ν_8, ν_{10}, and ν_{12} at 12, 23, 13, and 1 km mol^{-1}, respectively, but also more high intensity frequencies. Chief among these are the aforementioned antisymmetric B-H stretch of ν_3, as well as the ν_1 antisymmetric O-H stretch with an intensity of 133 km mol^{-1}, the ν_4 symmetric B-H stretch at 135 km mol^{-1}, and the ν_{13} symmetric B-O-H bend at 179 km mol^{-1}. For both molecules, the presence of these high intensity frequencies should help to facilitate their vibrational observation, if the molecules can be experimentally isolated in the gas phase. Further, the fact that there is little overlap between the frequencies of the most intense fundamentals means that the two can likely be disentangled if they are observed together in the same experiment.

The same is true for the rotational spectra of the two molecules also shown in Tables 3 and 4. Whereas the A_0 constant for BH_2OH is close to 172 GHz, that for BH_3OH_2 is much lower, near 87 GHz. Both molecules are near-prolate with κ values of -0.94 and -0.99 for BH_2OH and BH_3OH_2, respectively. Clearly BH_3OH_2 is much closer to prolate, as evidenced by the mere 452.6 MHz separation between its B_0 and C_0 constants, which are found at 17,269.0 and 16,816.4 MHz. Again, these are quite far away from those of BH_2OH, which are found experimentally at 30,470.22 and 25,812.73 MHz, suggesting that the two should be readily distinguished if observed in the same experiment. The quartic and sextic distortion coefficients for these two molecules are shown in Table S15 of the SI. The microwave spectra for BH_2OH and BH_3OH_2 are shown in Figures 5 and 6, respectively, and the rovibrational spectra for ν_2 of BH_2OH and ν_3 of BH_3OH_2 are shown in Figures 7 and 8.
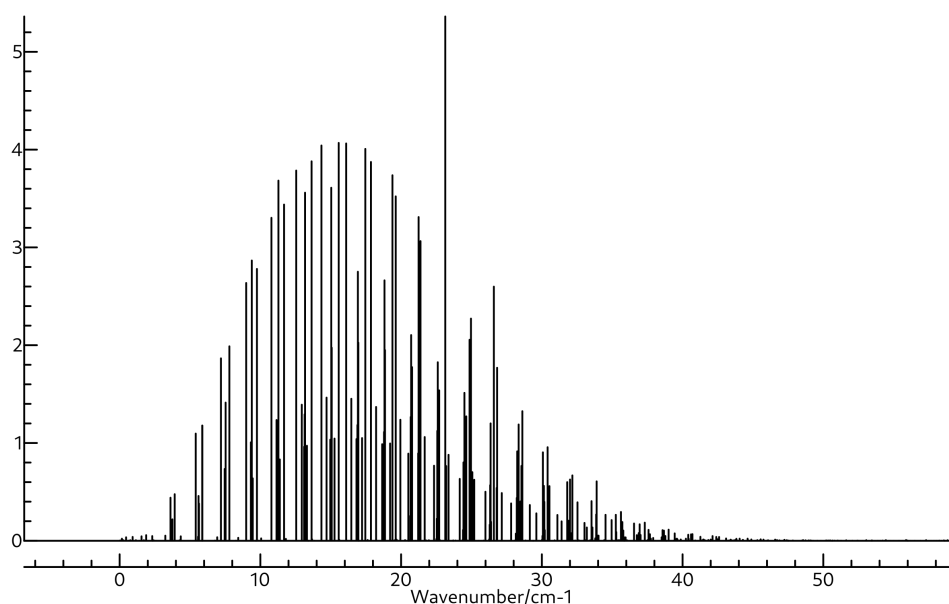

Figure 5. Simulated rotational spectrum of BH_2OH using A_0, B_0, and C_0 shown in Table 3, and Δ_J, Δ_{JK}, Δ_K, δ_J, δ_K, Φ_K, Φ_{KJ}, Φ_{JK}, and Φ_J shown in Table S15 at a temperature of 94 K with Lorentzian line shapes with FWHMs of 0.015 cm^{-1}.
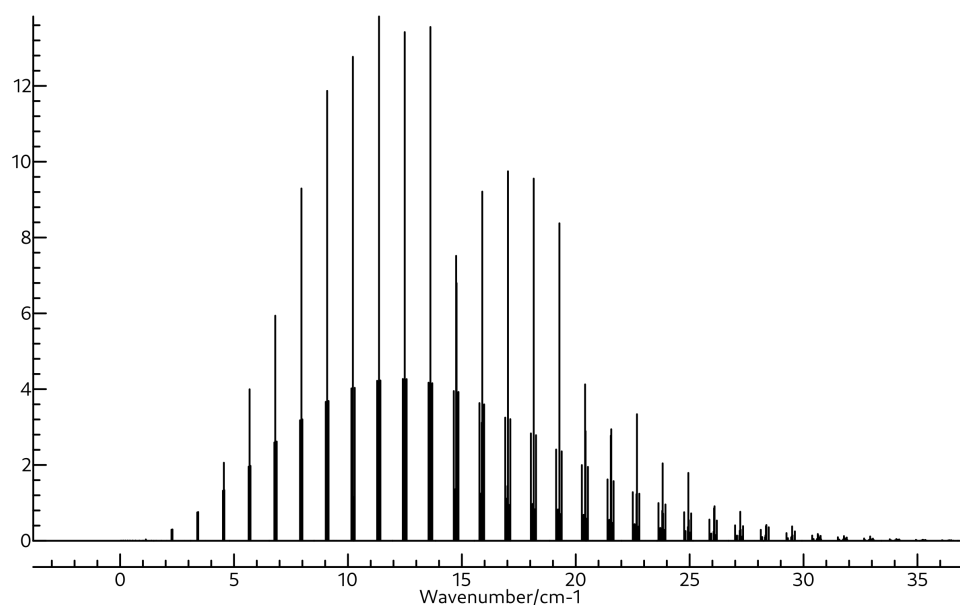
Figure 6. Simulated rotational spectrum of BH_3OH_2 using A_0, B_0, and C_0 shown in Table 4, and Δ_J, Δ_{JK}, Δ_K, δ_J, δ_K, Φ_K, Φ_{KJ}, Φ_{JK}, and Φ_J shown in Table S15 at a temperature of 94 K with Lorentzian line shapes with FWHMs of 0.015 cm^{-1}.
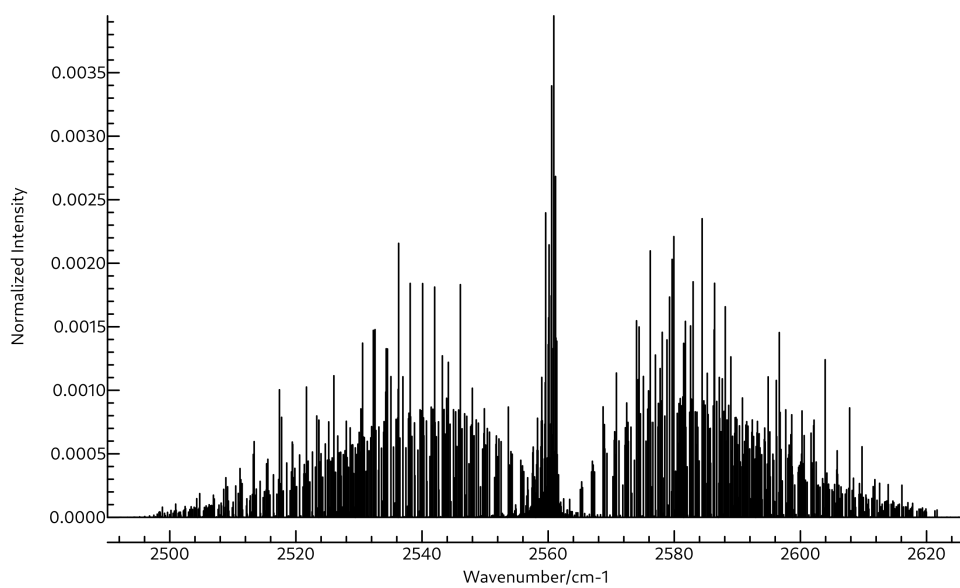
Figure 7. Simulated rovibrational spectrum of the first ν_2 transition of BH_2OH using A_0, B_0, C_0, A_2, B_2, and C_2 shown in Table 3, and Δ_J, Δ_{JK}, Δ_K, δ_J, δ_K, Φ_K, Φ_{KJ}, Φ_{JK}, and Φ_J shown in Table S15 at a temperature of 94 K with Lorentzian line shapes with FWHMs of 0.015 cm^{-1}.
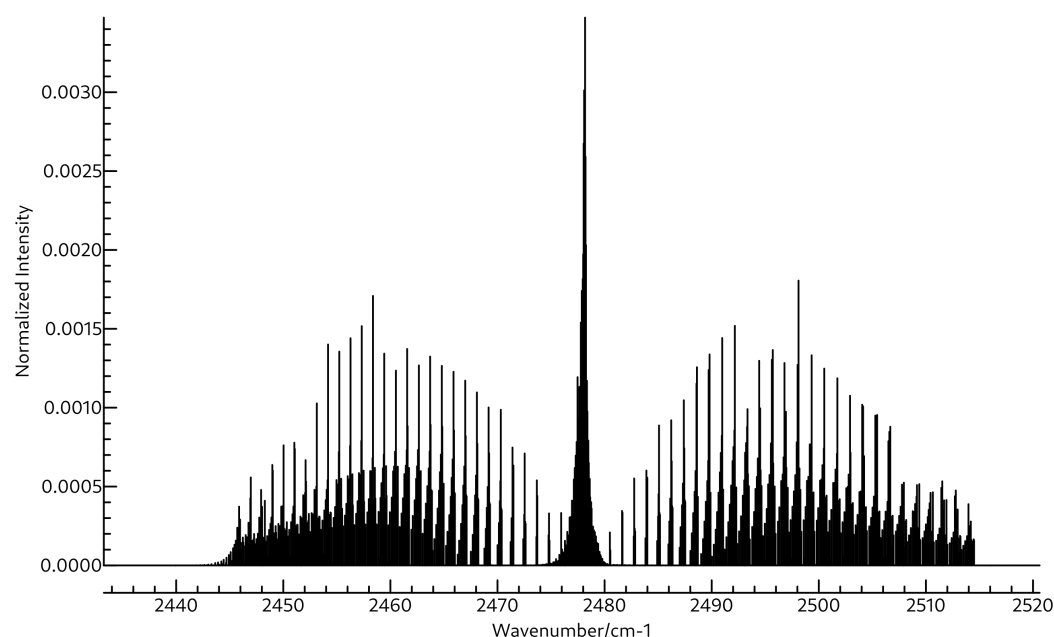
Figure 8. Simulated rovibrational spectrum of the first ν_3 transition of BH$_3$OH$_2$ using A_0, B_0, C_0, A_2, B_2, and C_2 shown in Table 4, and Δ_J, Δ_{JK}, Δ_K, δ_J, δ_K, Φ_K, Φ_{KJ}, Φ_{JK}, and Φ_J shown in Table S15 at a temperature of 94 K with Lorentzian line shapes with FWHMs of 0.015 cm^{-1}.

3.3. ^{10}B Isotopologues

All of the data discussed above are for the ^{11}B isotope. Given the relatively high isotopic abundance of ^{10}B, the computations are repeated for these isotopologues, and the results are reported in Tables S16–S55 of the SI. Overall, the trends are much the same as those observed for the ^{11}B variants. Namely, the F12-TZ-cCR fundamental frequencies are all within 2 cm^{-1} of the reported gas-phase values for borane [29] and HBO [30]; and the MAE for the principal rotational constants of borane is comparable to that for the ^{11}B variant at 252.3 MHz. The difference in the B_0 rotational constant of HBO is 15.1 MHz. However, the MAE for the vibrationally-averaged principal rotational constants of borinic acid is quite a bit higher than that of the ^{11}B isotopologue at 312.4 MHz. Most of the deviation is again in the A_0 constant, but this time even B_0 and C_0 have deviations over 100 MHz. Regardless, the good general agreement with the available experimental results suggests that the F12-TZ-cCR spectral data reported herein for ^{10}BH$_3$OH$_2$ and ^{10}BH$_2$OH should be reliable as well.

4. Conclusions

This work presents the most accurate rovibrational spectroscopic data for water borane, BH$_3$OH$_2$, and borinic acid, BH$_2$OH, currently available. The existence of gas-phase vibrational and rotational experimental data for the related borane, BH$_3$, and HBO molecules, as well as the vibrationally-averaged principal rotational constants of borinic acid, provide a wealth of benchmarking data for assessing the accuracy of the theoretical methods utilized for generating these novel data. In particular the recently developed F12-TZ-cCR QFF methodology performs substantially better than the more conventional F12-TZ methodology, which neglects explicit accounting for the effects of core correlation and scalar relativity. Both BH$_3$OH$_2$ and BH$_2$OH have several vibrational frequencies each with intensities over 100 km mol^{-1}, suggesting that these molecules will be readily observable in the infrared, if they can be experimentally isolated. Further, despite their structural similarity, these intense modes are sufficiently resolved that it should be possible to separate the two spectra if both molecules are produced in a single experiment. For BH$_2$OH, the most intense modes occur at 2561.6 (ν_2), 1352.8 (ν_4), and 1171.1 (ν_6) cm^{-1}, while those for BH$_3$OH$_2$ are found at 3704.8 (ν_1), 2488.4 (ν_3), 2452.3 (ν_4), 1176.8 (ν_9), and 528.4 (ν_{13}) cm^{-1}.

In terms of rotational spectra, BH_2OH possesses a substantial dipole moment of 1.51 D that helped to facilitate its previous experimental detection by microwave.png spectroscopy. Likewise, BH_3OH_2 has an enormous dipole moment of 4.24 D. As a result, it should be readily rotationally detectable as well, again if it can be isolated in the laboratory. Such isolation is of substantial importance due to the potential for both BH_3OH_2 and BH_2OH to be involved in the production of H_2 from water, which could be a promising route to clean alternative fuels. Regardless of the application, the highly-accurate theoretical rovibrational spectral data presented herein will help to guide future experimental investigations toward the detection of these molecules.

Supplementary Materials: The following are available online, Table S1–S14: Geometrical Parameters and Fermi Resonances for the [11]B Isotopologues, Table S15: Quartic and Sextic Distortion Coefficients for BH_2OH and BH_3OH_2, Tables S16–S55: Rovibrational Spectral Data for the [10]B Isotopologues, Tables S56–S58: Dipole Components.

References

1. Stephens, F.H.; Pons, V.; Baker, R.T. Ammonia-borane: The Hydrogen Source *par excellence*. *Dalton Trans.* **2007**, *25*, 2613–2626. [CrossRef] [PubMed]
2. Peng, B.; Chen, J. Ammonia Borane as an Efficient and Lightweight Hydrogen Storage Medium. *Energ. Environ. Sci.* **2008**, *4*, 479–483. [CrossRef]
3. Staubitz, A.; Robertson, A.P.M.; Manners, I. Ammonia-Borane and Related Compounds as Dihydrogen Sources. *Chem. Rev.* **2010**, *110*, 4079–4124. [CrossRef] [PubMed]
4. Sams, R.L.; Xantheas, S.S.; Blake, T.A. Vapor Phase Infrared Spectroscopy and Ab Initio Fundamental Anharmonic Frequencies of Ammonia Borane. *J. Phys. Chem. A* **2012**, *116*, 3124–3136. [CrossRef]
5. Weiss, H.G.; Shapiro, I. Mechanism of the Hydrolysis of Diborane in the Vapor Phase. *J. Am. Chem. Soc.* **1953**, *75*, 1221–1224. [CrossRef]
6. Nanayakkara, S.; Freindorf, M.; Tao, Y.; Kraka, E. Modeling Hydrogen Release from Water with Borane and Alane Catalysts: A Unified Reaction Valley Approach. *J. Phys. Chem. A* **2020**, *124*, 8978–8993. [CrossRef]
7. Swinnen, S.; Nguyen, V.S.; Sakai, S.; Nguyen, M.T. Calculations suggest facile hydrogen release from water using boranes and alanes as catalysts. *Chem. Phys. Lett.* **2009**, *472*, 175–180. [CrossRef]
8. Hirscher, M.; Autrey, T.; Orimo, S.I. Hydrogen Energy. *Chem. Phys. Chem.* **2019**, *20*, 1157. [CrossRef]
9. Tian, M.W.; Yuen, H.C.; Yan, S.R.; Huang, W.L. The Multiple Selections of Fostering Applications of Hydrogen Energy by Integrating Economic and Industrial Evaluation of Different Regions. *Int. J. Hydrogen Energy* **2019**, *44*, 29390–29398. [CrossRef]
10. Martin, A.; Agnoletti, M.F.; Brangier, E. Users in the Design of Hydrogen Energy Systems: A Systematic Review. *Int. J. Hydrogen Energy* **2020**, *45*, 11889–11900. [CrossRef]
11. Maghami, M.R.; Hassani, R.; Gomes, C.; Hizam, H.; Othman, M.L.; hammad Behmanesh, M. Hybrid Energy Management with Respect to a Hydrogen Energy System and Demand Response. *Int. J. Hydrogen Energy* **2020**, *45*, 1499–1509. [CrossRef]

12. Dreux, K.M.; McNamara, L.E.; Kelly, J.T.; Wright, A.M.; Hammer, N.I.; Tschumper, G.S. Probing Dative and Dihydrogen Bonding in Ammonia Borane with Electronic Structure Computations and Raman under Nitrogen Spectroscopy. *J. Phys. Chem. A* **2017**, *121*, 5884–5893. [CrossRef]

13. Westbrook, B.R.; Valencia, E.M.; Rushing, S.C.; Tschumper, G.S.; Fortenberry, R.C. Anharmonic Vibrational Frequencies of Ammonia Borane (BH_3NH_3). *J. Chem. Phys.* **2021**, *154*, 041104. [CrossRef]

14. Hess, N.J.; Bowden, M.E.; Parvanov, V.M.; Mundy, C.; Kathmann, S.M.; Schenter, G.K.; Autrey, T. Spectroscopic Studies of the Phase Transition in Ammonia Borane: Raman Spectroscopy of Single Crystal NH_3BH_3 as a Function of Temperature from 88 to 330K. *J. Chem. Phys.* **2008**, *128*, 034508. [CrossRef]

15. Paolone, A.; Teocoli, F.; Sanna, S.; Palumbo, O.; Autrey, T. Temperature Dependence of the Infrared Spectrum of Ammonia Borane: Librations, Rotations, and Molecular Vibrations. *J. Phys. Chem. C* **2013**, *117*, 729–734. [CrossRef]

16. Doerksen, E.S.; Fortenberry, R.C. A Coincidence Between Bond Strength, Atomic Abundance, and the Composition of Rocky Materials. *ACS Earth Space Chem.* **2020**, *4*, 812–816. [CrossRef]

17. Raghavachari, K.; Trucks, G.W.; Pople, J.A.; Replogle, E. Highly Correlated Systems: Structure, Binding Energy and Harmonic Vibrational Frequencies of Ozone. *Chem. Phys. Lett.* **1989**, *158*, 207–212. [CrossRef]

18. Adler, T.B.; Knizia, G.; Werner, H.J. A Simple and Efficient CCSD(T)-F12 Approximation. *J. Chem. Phys.* **2007**, *127*, 221106. [CrossRef] [PubMed]

19. Knizia, G.; Adler, T.B.; Werner, H.J. Simplified CCSD(T)-F12 Methods: Theory and Benchmarks. *J. Chem. Phys.* **2009**, *130*, 054104. [CrossRef]

20. Fortenberry, R.C.; Lee, T.J. Computational Vibrational Spectroscopy for the Detection of Molecules in Space. *Ann. Rep. Comput. Chem.* **2019**, *15*, 173–202.

21. Huang, X.; Valeev, E.F.; Lee, T.J. Comparison of One-Particle Basis Set Extrapolation to Explicitly Correlated Methods for the Calculation of Accurate Quartic Force Fields, Vibrational Frequencies, and Spectroscopic Constants: Application to H_2O, N_2H^+, NO_2^+, and C_2H_2. *J. Chem. Phys.* **2010**, *133*, 244108. [CrossRef]

22. Agbaglo, D.; Lee, T.J.; Thackston, R.; Fortenberry, R.C. A Small Molecule with PAH Vibrational Properties and a Detectable Rotational Spectrum: c-(C)C_3H_2, Cyclopropenylidenyl Carbene. *Astrophys. J.* **2019**, *871*, 236. [CrossRef]

23. Agbaglo, D.; Fortenberry, R.C. The Performance of CCSD(T)-F12/aug-cc-pVTZ for the Computation of Anharmonic Fundamental Vibrational Frequencies. *Int. J. Quantum Chem.* **2019**, *119*, e25899. [CrossRef]

24. Agbaglo, D.; Fortenberry, R.C. The Performance of Explicitly Correlated Wavefunctions [CCSD(T)-F12b] in the Computation of Anharmonic Vibrational Frequencies. *Chem. Phys. Lett.* **2019**, *734*, 136720. [CrossRef]

25. Westbrook, B.R.; Fortenberry, R.C. Anharmonic Frequencies of $(MO)_2$ & Related Hydrides for M = Mg, Al, Si, P, S, Ca, & Ti and Heuristics for Predicting Anharmonic Corrections of Inorganic Oxides. *J. Phys. Chem. A* **2020**, *124*, 3191–3204. [PubMed]

26. Valiev, R.R.; Nasibullin, R.T.; Cherepanov, V.N.; Baryshnikov, G.V.; Sundholm, D.; Ågren, H.; Minaev, B.F.; Kurtén, T. First-principles calculations of anharmonic and deuteration effects on the photophysical properties of polyacenes and porphyrinoids. *Phys. Chem. Chem. Phys.* **2020**, *22*, 22314–22323. [CrossRef] [PubMed]

27. Gardner, M.B.; Westbrook, B.R.; Fortenberry, R.C.; Lee, T.J. Highly-Accurate Quartic Force Fields for the Prediction of Anharmonic Rotational Constants and Fundamental Vibrational Frequencies. *Spectrochim. Acta A* **2021**, *248*, 119184. [CrossRef]

28. Watrous, A.G.; Westbrook, B.R.; Fortenberry, R.C. F12-TZ-cCR: A Methodology for Faster and Still Highly-Accurate Quartic Force Fields. *J. Phys. Chem. A* **2021**, submitted. [CrossRef]

29. Kawaguchi, K. Fourier Transform Infrared Spectroscopy of BH_3 with the First Identification of the ν_4 Band. *J. Molec. Spectrosc.* **2020**, *373*, 111352. [CrossRef]

30. Kawashima, Y.; Endo, Y.; Hirota, E. Microwave Spectrum, Molecular Structure, and Force Field of HBO. *J. Molec. Spectrosc.* **1989**, *133*, 116–127. [CrossRef]

31. Kawashima, Y.; Takeo, H.; Matsumura, C. Microwave Spectrum of Borinic Acid BH_2OH. *J. Chem. Phys.* **1981**, *74*, 5430–5435. [CrossRef]

32. Werner, H.J.; Knowles, P.J.; Manby, F.R.; Black, J.A.; Doll, K.; Heßelmann, A.; Kats, D.; Köhn, A.; Korona, T.; Kreplin, D.A.; et al. MOLPRO, Version 2020.1, a Package of *ab Initio* Programs. 2020. Available online: http://www.molpro.net (accessed on 14 September 2021).

33. Peterson, K.A.; Adler, T.B.; Werner, H.J. Systematically Convergent Basis Sets for Explicitly Correlated Wavefunctions: The Atoms H, He, B-Ne, and Al-Ar. *J. Chem. Phys.* **2008**, *128*, 084102. [CrossRef] [PubMed]

34. Hill, J.G.; Mazumder, S.; Peterson, K.A. Correlation Consistent Basis Sets for Molecular Core-Valence Effects with Explicitly Correlated Wave Functions: The Atoms B-Ne and Al-Ar. *J. Chem. Phys.* **2010**, *132*, 054108. [CrossRef] [PubMed]

35. Douglas, M.; Kroll, N. Quantum Electrodynamical Corrections to the Fine Structure of Helium. *Ann. Phys.* **1974**, *82*, 89–155. [CrossRef]

36. Jansen, G.; Hess, B.A. Revision of the Douglas-Kroll Hamiltonian. *Phys. Rev. A* **1989**, *39*, 6016–6017. [CrossRef]

37. Frisch, M.J.; Trucks, G.W.; Schlegel, H.B.; Scuseria, G.E.; Robb, M.A.; Cheeseman, J.R.; Scalmani, G.; Barone, V.; Petersson, G.A.; Nakatsuji, H.; et al. *Gaussian 16 Revision C.01*; Gaussian Inc.: Wallingford, CT, USA, 2016.

38. Møller, C.; Plesset, M.S. Note on an Approximation Treatment for Many-Electron Systems. *Phys. Rev.* **1934**, *46*, 618–622. [CrossRef]

39. Kendall, R.A.; Dunning, T.H.; Harrison, R.J. Electron Affinities of the First-Row Atoms Revisited. Systematic Basis Sets and Wave Functions. *J. Chem. Phys.* **1992**, *96*, 6796–6806. [CrossRef]

40. Yu, Q.; Bowman, J.M.; Fortenberry, R.C.; Mancini, J.S.; Lee, T.J.; Crawford, T.D.; Klemperer, W.; Francisco, J.S. The Structure, Anharmonic Vibrational Frequencies, and Intensities of $NNHNN^+$. *J. Phys. Chem. A* **2015**, *119*, 11623–11631. [CrossRef]

41. Finney, B.; Fortenberry, R.C.; Francisco, J.S.; Peterson, K.A. A Spectroscopic Case for SPSi Detection: The Third-Row in a Single Molecule. *J. Chem. Phys.* **2016**, *145*, 124311. [CrossRef]

42. Westbrook, B.R.; Patel, D.J.; Dallas, J.D.; Swartzfager, G.C.; Lee, T.J.; Fortenberry, R.C. Fundamental Vibrational Frequencies and Spectroscopic Constants of Substituted Cyclopropenylidene (*c*-C_3HX, X=F,Cl,CN). *J. Phys. Chem. A* **2021**, in press. [CrossRef]

43. Watrous, A.G.; Westbrook, B.R.; Davis, M.C.; Fortenberry, R.C. Vibrational and Rotational Spectral Data for Possible Interstellar Detection of AlH_3OH_2, SiH_3OH, and SiH_3NH_2. *Mon. Not. R. Astron. Soc.* **2021**, *508*, 2613–2619. [CrossRef]

44. Watrous, A.G.; Davis, M.C.; Fortenberry, R.C. Pathways to Detection of Strongly-Bound Inorganic Species: The Vibrational and Rotational Spectral Data of AlH2OH, HMgOH, AlH2NH2, and HMgNH2. *Front. Astron. Space Sci.* **2021**, *8*, 1–11. [CrossRef]

45. Allen, W.D.; Császár, A.G.; Szalay, V.; Mills, I.M.; Horner, D.A. *INTDER* 2005 Is a General Program Written by W. D. Allen and Coworkers, Which Performs Vibrational Analysis and Higher-Order Non-Linear Transformations. 2005. Available online: https://r410berry.com/static/media/INTDER05_Manual.09dde4b6.pdf (accessed on 15 September 2021).

46. Mills, I.M. Vibration-Rotation Structure in Asymmetric- and Symmetric-Top Molecules. In *Molecular Spectroscopy—Modern Research*; Rao, K.N., Mathews, C.W., Eds.; Academic Press: New York, NY, USA, 1972; pp. 115–140.

47. Gaw, J.F.; Willets, A.; Green, W.H.; Handy, N.C. SPECTRO: A Program for the Derivation of Spectrscopic Constants from Provided Quartic Force Fields and Cubic Dipole Fields. In *Advances in Molecular Vibrations and Collision Dynamics*; Bowman, J.M., Ratner, M.A., Eds.; JAI Press, Inc.: Greenwich, CT, USA, 1991; pp. 170–185.

48. Watson, J.K.G. Aspects of Quartic and Sextic Centrifugal Effects on Rotational Energy Levels. In *Vibrational Spectra and Structure*; During, J.R., Ed.; Elsevier: Amsterdam, The Netherlands, 1977; pp. 1–89.

49. Papousek, D.; Aliev, M.R. *Molecular Vibration-Rotation Spectra*; Elsevier: Amsterdam, The Netherlands, 1982.

50. Martin, J.M.L.; Taylor, P.R. Accurate *ab Initio* Quartic Force Field for *trans*-HNNH and Treatment of Resonance Polyads. *Spectrochim. Acta A* **1997**, *53*, 1039–1050. [CrossRef]

51. Martin, J.M.L.; Lee, T.J.; Taylor, P.R.; François, J.P. The Anharmonic Force Field of Ethylene, C_2H_4, by Means of Accurate *ab Initio* Calculations. *J. Chem. Phys.* **1995**, *103*, 2589–2602. [CrossRef]

52. Western, C.M. PGOPHER, A Program for Simulating Rotational, Vibrational and Electronic Spectra. *J. Quant. Spectrosc. Radiat. Transf.* **2017**, *186*, 221–242. [CrossRef]